Surface modes in air-core photonic band-gap fibers

James A. West, Charlene M. Smith, Nicholas F. Borrelli, Douglas C. Allan, and Karl W. Koch

Sullivan Park, Corning Incorporated, Corning, NY 14831
westja@corning.com

http://www.corning.com

Abstract: We present a detailed description of the role of surface modes in photonic band-gap fibers (PBGFs). A model is developed that connects the experimental observations of high losses in the middle of the transmission spectrum to the presence of surface modes supported at the core-cladding interface. Furthermore, a new PBGF design is proposed that avoids these surface modes and produces single-mode operation.

OCIS codes: (060.0060) Fiber optics and optical communications; (060.2280) Fiber design and fabrication; (060.2430).

References and links

1. N. Venkataraman, M.T. Gallagher, D. Müller, Charlene M. Smith, J. A. West, K. W. Koch, and J. C. Fajardo, "Low-Loss (13 dB/km) Air-Core Photonic Band-Gap Fibre", *Proceedings of ECOC 2002* (Copenhagen, Denmark, 2002) PD1.1.
2. C. M. Smith, N. Venkataraman, M. T. Gallagher, D. Müller, J. A. West, N. F. Borrelli, D. C. Allan and K. W. Koch, "Low-loss hollow-core silica/air photonic bandgap fibre," Nature **424**, 657-659 (2003).
3. K. Saitoh and M. Koshiba, "Leakage loss and group velocity dispersion in air-core photonic bandgap fibers," Opt. Express **11**, 3100-3109 (2003), http://www.opticsexpress.org/abstract.cfm?URI=OPEX-11-23-3100.
4. K. Saitoh, N. A. Mortensen, and M. Koshiba, "Air-core photonic band-gap fibers: the impact of surface modes," Opt. Express **12**, 394-400 (2004), http://www.opticsexpress.org/abstract.cfm?URI=OPEX-12-3-394.
5. D. C. Allan, et al., *Photonic Crystals and Light Localization in the 21st Century*, C. M. Soukoulis (ed.), (Kluwer Academic Press, The Netherlands, 2001), pp. 305-320.
6. D. C. Allan, N. F. Borrelli, M. T. Gallagher, D. Müller, C. M. Smith, N. Venkataraman, J. A. West, P. Zhang, K.W. Koch, "Surface modes and loss in air-core photonic bandgap fibers," in *Photonic Crystal Materials and Devices*, Ali Adibi, Axel Scherer, and Shawn Yu Lin;, eds. Proc. SPIE **5000**, p. 161-174 (2003).
7. J. D. Joannopoulos, R. D. Meade and J. N. Winn, *Photonic Crystals* (Princeton University Press, Princeton, N.J., 1995), pp. 73-76.
8. P. Yeh, *Optical Waves in Layered Media*,(John Wiley & Sons, New York, N.Y., 1988) pp. 337-345.
9. D. C. Allan, N.F. Borrelli, J. C. Fajardo, K. W. Koch, and J. A. West. Corning Incorporated "Optimized defects in band-gap waveguides," U.S. Pat. Appl. 20020136516-A1. February 4 2002.
10. S. G. Johnson, M. Ibanescu, M. Skorobogatiy, O. Weisberg, J. D. Joannopoulos, and Y. Fink, "Perturbation theory for Maxwell's equations with shifting material boundaries," Phys. Rev. E **65**, 66611 (2002).
11. M. Skorobogatiy, S. A. Jacobs, S. G. Johnson, and Y. Fink, "Geometric variations in high index-contrast waveguides, coupled mode theory in curvilinear coordinates," Opt. Express **10**, 1227-1243 (2002), http://www.opticsexpress.org/abstract.cfm?URI=OPEX-10-21-1227.
12. A. W. Snyder and J. D. Love, *Optical Waveguide Theory* (Kluwer Academic Publishers, Boston, MA, 2000), Eq. 31-50a.
13. S. G. Johnson and J. D. Joannopoulos, "Block-iterative frequency-domain methods for Maxwell's equations in a planewave basis," Opt. Express **8**, 173-190 (2001), http://www.opticsexpress.org/abstract.cfm?URI=OPEX-8-3-173.
14. B. J. Mangan, L. Farr, A. Langford, P. J. Roberts, D. P. Williams,F. Couny, M. Lawman, M. Mason, S. Coupland, R. Flea and H. Sabert, "Low loss (1.7 dB/km) hollow core photonic bandgap fiber," *Proceedings of OFC 2004*, (OSA, Los Angeles, CA, 2004) PDP24.

#3956 - $15.00 US Received 2 March 2004; revised 28 March 2004; accepted 30 March 2004

1. Introduction

Hollow-core photonic band-gap fibers (PBGFs) are typically made up of a periodic array of air holes in glass, surrounding an air core. These fibers have attracted considerable interest because they hold the promise of exhibiting lower attenuation and lower nonlinearity than conventional glass-core fibers. The potential for lower attenuation derives from the lower absorption and lower Rayleigh scattering of air relative to glass. In practice however, the attenuation of small-core PBGFs is still far from the losses typical in standard single-mode optical fiber (~0.2 dB/km), with a low value of 13 dB/km reported in 2002 [1,2].

Photonic band-gap fibers rely on the interference of light reflected from the periodic structures in the cladding. Among the most commonly suggested loss mechanisms in such fibers is tunneling or confinement loss due to the exponential tail of the mode field extending beyond the finite extent of the cladding. Tunneling loss is not unique to PBGFs and is present in all conventional optical fibers with high-index polymer coatings. Recent work has examined the impact of air-filling fraction and the number of rows of air holes on tunneling loss in PBGFs [3,4]. These calculations suggest that tunneling losses of <0.1 dB/km should be achievable in 10-row, high air-fill structures (>94%) with single-mode cores, thus reported attenuations do not appear to be limited by this mechanism. Consequently, as is assumed in the study of conventional optical fiber, we will treat the theoretically "leaky" core modes as true guided modes. Experimental confirmation of the present tunneling calculations will require the fabrication of fibers with significantly lower losses or fewer rows of air holes.

Several other PBGF loss mechanisms have been suggested but, unlike tunneling loss, none of these has been studied in sufficient detail to quantify the contribution to the overall loss. These additional sources of loss can be characterized as resulting from either absorption or from mode coupling. Although absorption will ultimately play a role in determining the lower limit on PBGF attenuation, in fibers made from high-quality waveguide-grade silica in a dry inert environment, there is currently no evidence of absorption loss for modes confined to the core. Thus we attribute most of the observed loss to the general category of mode coupling in which perturbations along the fiber couple light between the guided and leaky modes. These perturbations may be due to surface roughness, axial variations of the fiber scale or structure, stress, bending, twisting or other effects that change the index profile along the direction of propagation. In this paper we do not focus on the perturbations themselves, but instead deal with the consequence of such perturbations.

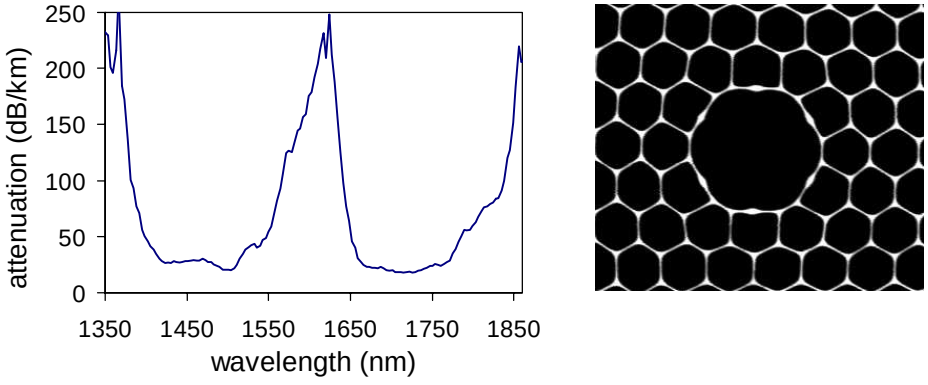

Fig. 1. (a) Optical attenuation as a function of wavelength for the 65-m long air-core PBGF using a conventional cut-back technique [2]. The loss feature between 1550 and 1650 nm is attributed to surface modes. (b) SEM of the air-silica PBGF profile, truncated to show central core defect and first rings of holes of microstructured cladding. The parameters are described in Ref. [2].

#3956 - $15.00 US Received 2 March 2004; revised 28 March 2004; accepted 30 March 2004

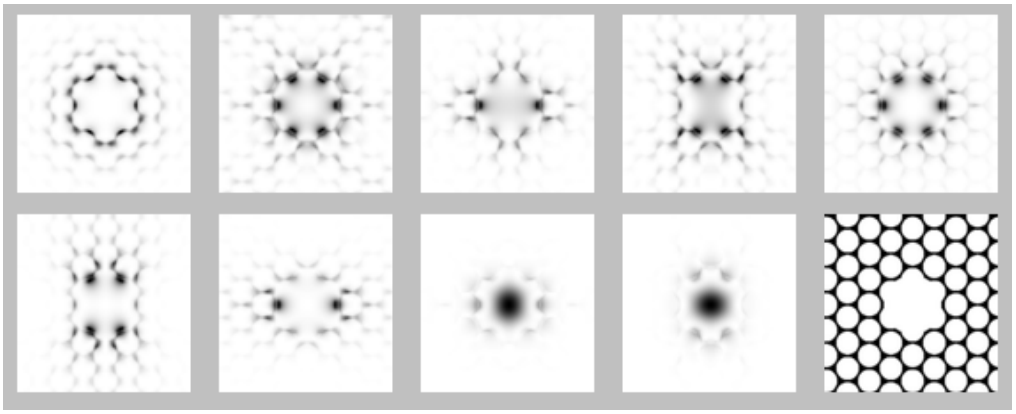

Fig. 2. Modal plots of 7 surface modes, and 2 core modes that lie within the band gap of an undistorted silica structure (shown at lower right) with defect radius of R_d=1.15Λ and air-hole radius of r=0.45Λ. Note that the core mode has some spatial overlap with the surface modes.

Similar to standard optical fibers, a PBGF is expected to have a finite number of well confined core modes and an essentially infinite number of leaky cladding and radiation modes. In the ideal case, the core modes have nearly all of their energy in the air and perturbations of the silica structure only weakly couple the core modes to the cladding modes with which they have the largest spatial overlap in the perturbed region. However, in some PBGFs, a second type of core mode has been identified and is referred to as a surface mode [2,5,6]. Such surface modes are not unexpected in periodic structures [7,8] but in a PBGF the fixed relationship between the location of the surface and the lattice structure removes the usual degree of freedom that is used to control these modes. Although surface modes are unavoidable in most PBGF designs, in Section 4 we show a structure that reduces their impact on core transmission.

In the following sections we summarize a coupled-mode description of surface modes that has been presented previously and justify the analysis with modal overlap calculations and experimental results of attenuation and modal profiles. We conclude by presenting a design that reduces the impact of surface modes in a single-mode PBGF.

2. Coupled-mode description of surface-mode losses

Although surface modes were first reported in PBGFs several years ago [5], a more complete description has emerged only recently [2,6]. The attenuation spectrum of an air-core fiber having a band gap of roughly 450 nm shows a region of high loss in the spectral region between 1550 and 1650 nm (see Fig. 1). A comparison of the experimental and computational results led to the suggestion that this high-loss region is related to coupling between the core modes and extended modes supported by the photonic band-gap structure [2,6]. Specifically, it was proposed that surface modes, by coupling to the core modes as well as to the lossy extended modes, provide a loss mechanism for core modes. To understand this loss mechanism it is important to first understand the surface modes themselves.

For the case of a planar interface of a semi-infinite periodic structure, the nature of the surface modes is well understood [7,8]. These surface modes, which decay exponentially into both the periodic structure and free space, can be manipulated by changing the location of the surface relative to the periodicity of the lattice. However, in the case of a PBGF, the surface is defined by the core radius, producing a finite circular interface rather than infinite planar interface. This surface supports modes whose frequencies lie within the band gap and so are localized near the core but, unlike the true core modes, most of the intensity is in the glass surrounding the core (see Fig. 2 and Fig. 7). If the amount of glass around the core is reduced, the energies of these modes increase moving them into the band gap while the energies of the

#3956 - $15.00 US Received 2 March 2004; revised 28 March 2004; accepted 30 March 2004

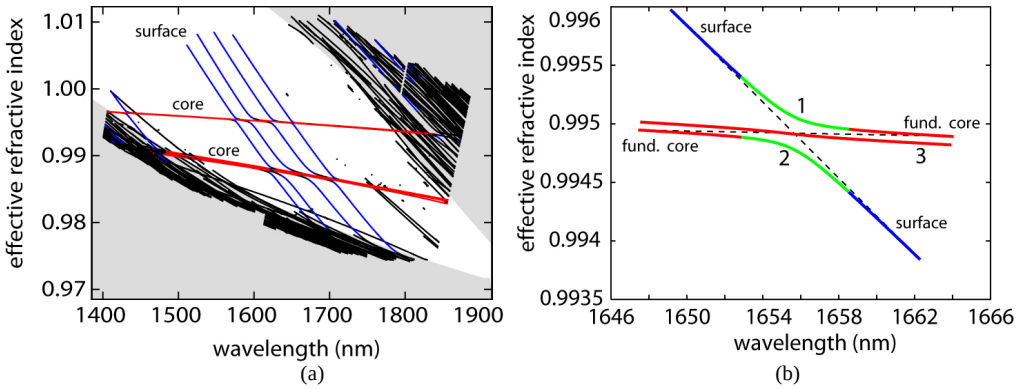

Fig. 3. (a) Calculated dispersion of air-core modes and band-gap modes for the fiber profile in Fig. 1(b). The black symbols represent modes of the cladding structure. The blue symbols represent modes whose intensity is predominantly on the surface of the air-core defect. The red symbols represent the modes with a majority of their intensity within the air-core defect. The fundamental air-core modes have a higher effective index than the higher-order air-core modes. The shaded region indicates the continuum regions surrounding the band gap. (b) Expanded view of core-surface-mode avoided crossing near 1655 nm. Red indicates core-like modes, blue indicates surface-like modes and modes which cannot be accurately approximated by either a core or surface mode are colored green. The dashed lines show the approximate core and surface modes used in the supermode theory. The numbers are used in Figs. 6 and 7 to refer to the modes.

true core modes remain relatively unchanged. Over some range of core radii the surface and core modes interact and their fields have significant overlap in the silica regions. This overlap allows axial perturbations in the fiber structure to couple light between the core and surface modes. The more extended nature of the surface modes leads to a significant overlap with a continuum of extended modes in the cladding. This coupling to the extended modes is the essence of the argument that the surface modes contribute to fiber attenuation. We shall refer to this as the surface-mode loss mechanism.

It has been suggested that the surface modes can be controlled by changing the radius of the waveguide [9] but the traditional requirement to maintain single-mode operation limits the range over which the core radius can be varied. This is examined in more detail in Section 4 in which we present optimal fiber designs chosen to avoid surface modes.

To explore the role of surface modes in a real fiber, we show in Fig. 3(a) a map of the band gap obtained by plotting the calculated effective refractive index of the modes of the low-loss fiber shown in Fig. 1. Details of the calculation can be found in Ref. 2. The calculated band gap spans the wavelength region from 1400 nm to 1850 nm, in good agreement with the experimental result. Six air-core modes are shown: two polarizations of a fundamental core mode and four, nearly degenerate, higher-order core modes. In addition to the air-core modes there are also four modes that cross the air-core modes within the band gap; these modes are nearly degenerate with the core modes between 1575 nm and 1710 nm. These are the surface modes described above. Note that their positions lie within the experimentally determined high-loss region of the fiber.

An analysis of the expected losses associated with surface modes was previously described [6]. A coupled-mode theory approximates the interaction between each surface mode and core mode. Instead of dealing with the true modes of the system, we assume that they are approximated by a lossless core mode and a lossy surface mode. The true modes of the system, often referred to as *supermodes*, can be described by linear superpositions of the core and surface modes. A loss term $(-\gamma A_j)$ is introduced into the coupled equations to address the proposed surface-mode loss mechanism. The loss rate γ, characterizes that rate at which energy is coupled out of the surface modes and thus out of the coupled system. With this loss term, the coupled-mode equations are simply:

#3956 - $15.00 US Received 2 March 2004; revised 28 March 2004; accepted 30 March 2004

$$\frac{dA_i}{dz} = -i\kappa_{ij} A_j e^{i\Delta\beta_{ij} z} \tag{1}$$

$$\frac{dA_j}{dz} = -i\kappa_{ij}^{*} A_i e^{-i\Delta\beta_{ij} z} - \gamma_j A_j \tag{2}$$

Here A_i and A_j are the complex field amplitudes of the core or surface mode, respectively, κ_{ij} describes coupling between the modes, $\Delta\beta_{ij}$ is the difference in wavevectors between the two coupled modes, and z is the distance along the fiber. The loss term represents a continuous loss of power from the surface mode due to assumed coupling to extended modes through small structural perturbations. This is motivated in more detail in Section 3.

In Ref. 6, the coupled-mode equations describing core mode i and surface mode j are shown to have core-mode solutions that decay exponentially with an attenuation coefficient given by:

$$\alpha_{ij}(\text{dB/km}) \approx \frac{20}{\ln(10)} \frac{\gamma_j \left|\kappa_{ij}\right|^2}{\left(\Delta\beta_{ij}\right)^2} \tag{3}$$

where γ_j, κ_{ij} and $\Delta\beta_{ij}$ are in km^{-1}. Here the wavelength dependence of $\Delta\beta_{ij}$ leads to an approximately Lorentzian loss spectrum. We assume that, in this approximation, κ_{ij} and γ_j are essentially independent of wavelength.

From Fig. 3(b), it is obvious that $\Delta\beta_{ij}(\lambda)$ has a minimum in the vicinity of each avoided crossing and thus the loss is greatest at these wavelengths. Near the avoided crossings the difference in propagation constants is shown to be approximately quadratic:

$$\left(\Delta\beta_{ij}\right)^2 = \left(\frac{2\pi}{\lambda}\right)^2 \left(\Delta n_{eff,ij}\right)^2 \tag{4}$$

$$\Delta n_{eff,ij} = \Delta n_{\min,ij} + \Lambda s_{ij} (\lambda - \lambda_{\min,ij})^2 \tag{5}$$

where Λ is the pitch of the lattice, $\lambda_{min,ij}$ is the wavelength of the avoided crossing, $\Delta n_{min,ij}$ is the minimum difference in the supermode effective indices at the avoided crossing, and s_{ij} is the difference in slopes of the n_{eff} of the uncoupled modes (see dashed lines in Fig. 3(b)):

$$s_{ij} = \frac{dn_{eff,i}}{d\tilde{\omega}} - \frac{dn_{eff,j}}{d\tilde{\omega}}, \tag{6}$$

where $\tilde{\omega}$ is the scaled frequency Λ/λ. The relationship between the coupling coefficient κ_{ij} and $\Delta n_{min,ij} = \kappa_{ij}\lambda_{min,ij}/\pi$ allows us to obtain values for the coupling coefficients from calculations of the avoided crossings such as the one shown in Fig. 3(b).

The individual avoided crossings in Fig. 3(a) were analyzed and the values of the various parameters were extracted from the crossings. Assuming that the six air-core modes are launched with initial intensities $I_i(z=0)$, the overall loss spectrum on a fiber of length L can be computed by:

$$\alpha(\lambda) = -\frac{10}{L} * \log_{10}\left(\frac{\sum_i I_i(0) 10^{-\sum_j \alpha_{ij}(\lambda) L}}{\sum_i I_i(0)} \right) \tag{7}$$

where the summation j is over the surface modes that are coupled to core mode i. The multimode nature of the launch leads to a complicated expression in which the resulting loss spectrum is dominated by the lowest-loss mode at each wavelength. Because of this, individual loss terms α_{ij} with large peak losses result in a total attenuation coefficient with significantly smaller peak attenuation and broader-than-expected tails.

The comparison between the experimental loss data and the results of the model are shown in Fig. 4(a). To fit the experimental data we make a number of assumptions. We

#3956 - $15.00 US Received 2 March 2004; revised 28 March 2004; accepted 30 March 2004

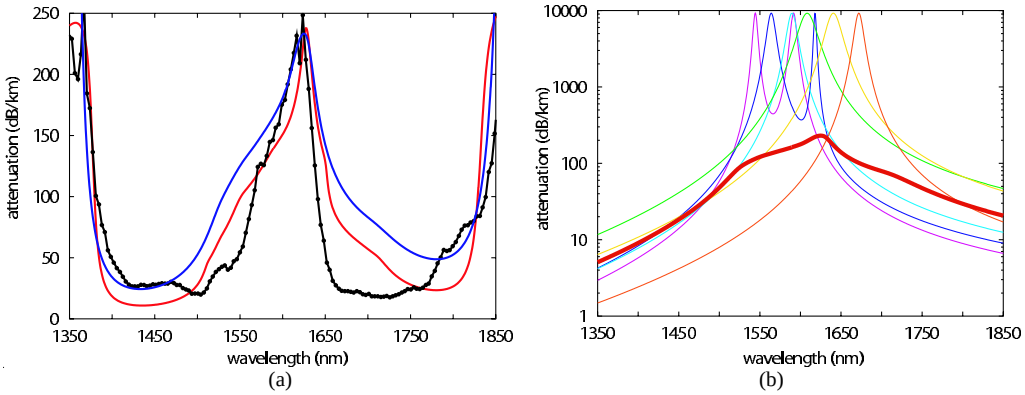

Fig. 4. (a) Experimental (black line with points) and calculated attenuation spectra of the fiber shown in Fig. 1. The solid blue curve assumes no change in the fiber scale with γ=4250 km^{-1}; the red curve models a 4% variation in the fiber scale over the 65-meter length with γ=1750 km^{-1}. The band edges are approximated by Lorentzians to illustrate the possible impact of the band edges on attenuation. (b) Individual loss contributions α_{ij} (thin, multicolored lines) compared to the overall loss coefficient α (heavy red line) for a fiber with no scale variation .

include two additional Lorentzians simply to indicate the possible impact of the band edges. We introduce an overall shift of -2% in the wavelengths predicted from Fig. 3(a). We justify this because of the uncertainty of the thresholding used to convert the SEM image into an index profile for the calculation. We let γ be a free parameter that is assumed to be constant for all surface modes. Finally, we assume that the multiple core modes are launched equally.

Under the above assumptions the fit in Fig. 4(a) is reasonable although the calculated tails of the surface-mode loss extend further than is observed in the data. This is because the individual coefficients α_{ij} have very much larger peak losses than the cumulative loss coefficient. This is dramatically illustrated in Fig. 4(b). To achieve the observed peak surface-mode loss of ~240 dB/km, γ must have a value of 4250 km^{-1} or 37000 dB/km giving the α_{ij} peak values of 9000 dB/km. These values can be lowered significantly if we consider the impact of simple scale variations on the attenuation. If we ignore mode coupling, scale variations along the fiber simply shift the peak wavelengths of the α_{ij}. In this approximation, the fiber transmission can be thought of as a filter whose center wavelength varies along the fiber. For a linear fractional scale variation x along the fiber, this may be modeled by assuming that:

$$\lambda_{\min,ij}(z) = \lambda_{\min,ij}(0)(1 + z\,x / L) \tag{8}$$

When such a modification is introduced into the model, the required value of γ drops and the tails of the Lorentzians decrease as shown by the red curve in Fig. 4(a). The 4% variation used to model the red curve in Fig. 4(a) is comparable to the axial variation observed in various cross-sections of this fiber. We note that in the absence of mode-coupling this scale variation can be modeled as a linear system and any variation can be reduced to a monotonic function of fiber length.

As final evidence of the predictive ability of our model, in Fig. 5(a) we plot the fraction of transmitted light in the two fundamental core modes (red curve) or the four higher-order modes (blue curve) relative to the total light transmitted. These curves would suggest that an experimental measurement of the modes transmitted through the fiber would show only higher-order modes in the range from 1530 to 1630 nm. The results of such a measurement are shown in the movie of Fig. 5(b) and indeed they show the predicted behavior almost exactly. The modal images were captured on an InGaAs focal-plane array using a high-brightness EELED source and an optical spectrum analyzer as a 10-nm tunable filter. In the region around 1600 nm, the fundamental mode could not be detected regardless of the launching conditions while in the low-loss regions it was possible to observe the multi-mode

#3956 - $15.00 US Received 2 March 2004; revised 28 March 2004; accepted 30 March 2004

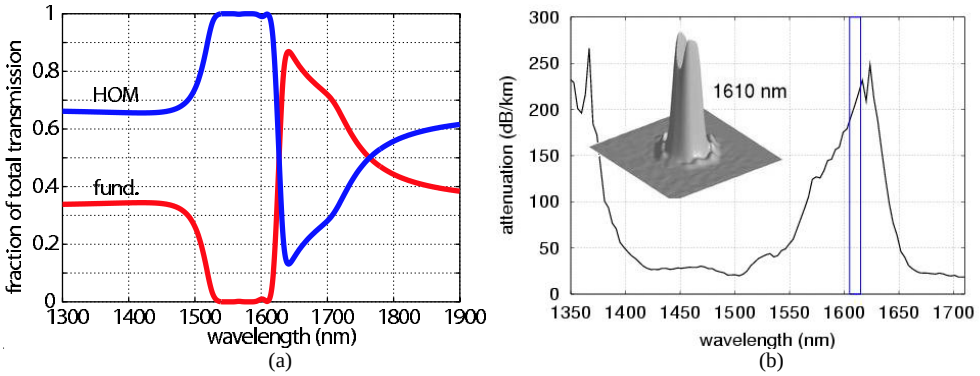

Fig. 5. (a) Fraction of transmitted light in the two fundamental core modes (red) or the four higher-order modes (blue) relative to the total light transmitted calculated using the same model as the red curve in Fig. 4(a). Between 1530 and 1630 nm, almost 100% of the light transmitted is in the higher order modes. (b) (750 Kb) Movie of a spectrally resolved experimental measurement of the spatial distribution of modes of the fiber in Fig. 1. Note the "surface-mode" character of the mode between 1500 and 1650 nm and also that the light is transmitted in a higher-order mode between 1570 and 1630 nm in agreement with the predictions of the surface-mode theory.

nature of the field with varying launch conditions. This lack of sensitivity to the launch conditions is also seen in the model and can be explained by the large attenuation coefficients of the individual modes. Even if only 1% of a higher-order mode is launched, over a range of wavelengths its contribution at the end of the fiber is far greater than that of a fundamental mode which sees 100X greater attenuation due to surface-mode coupling.

3. Overlap calculations of core, surface and extended modes

The previous section described the loss characteristics resulting from the coupling between a core mode and a lossy surface mode. In this section we motivate how perturbations along the fiber couple the surface mode to a continuum of cladding modes leading to loss in the surface mode. Although we believe that coupling to cladding modes is the dominant contribution to the loss coefficient γ, the surface modes have been shown to be leakier than core modes [4] and so tunneling losses may also contribute. However, in the vicinity of the avoided crossings the modeling of Ref. 4 shows levels of loss < 1dB/km, a value that would be further reduced to a negligible level if the modeling had used the 8 rings of holes reported for the experimental fiber [2].

The "coupling" described in the previous section can be thought of as a supermode theory in which the true modes of the structure can be treated as combinations of "modes" of just the air-core and "modes" of just the surface. Away from the avoided crossings one set of the true modes are well approximated by the "modes" of core while another set of true modes is well approximated by the "modes" of the surface. However, near the crossing wavelengths, the true modes are best approximated by symmetric and anti-symmetric linear combinations of the two "modes", one core "mode" and one surface "mode", involved in the interaction. In this supermode theory, the coupling strength simply characterizes the bandwidth of the coupling region and does not result in actual coupling between the true modes of the structure nor does it lead to loss.

The loss coefficient γ comes from a more traditional form of coupled-mode theory in which structural changes lead to perturbations in the modes. The electric field in a given cross-section can always be described by a local superposition of the guided and extended modes of that cross-section. If the structure changes, the modes will change, and the field must be re-expressed in this new basis of local modes. For small perturbations, the set of new modes can generally be matched one-for-one to the original set of modes with small changes

#3956 - $15.00 US Received 2 March 2004; revised 28 March 2004; accepted 30 March 2004

in mode energy and mode structure, so core and surface modes of the unperturbed structure can be identified with corresponding core and surface modes of the perturbed structure. Loss is a consequence of the perturbation, leading to light being coupled from the guided core and surface modes to the extended or radiation modes. To investigate coupling loss we could calculate the modes of both the perturbed and unperturbed structure and simply re-express the original core mode in this new basis of modes. Alternatively we can turn to perturbation theory to calculate the coupling coefficients that described the coupling of light into these new modes of the structure.

PBGFs pose a difficult problem for perturbation theory because of the presence of high-contrast dielectric structures with step-function spatial changes in the dielectric [10,11]. However, we are looking only for insight into the coupling process and so we apply standard perturbation theory for waveguides and draw our conclusions with the knowledge of this difficulty. Following the standard approach we can define the coupling coefficients by [12]:

$$C_{12} \propto \int_A (\varepsilon - \tilde{\varepsilon}) \left\{ \mathbf{E}_{t1}^* \cdot \mathbf{E}_{t2} + \frac{\tilde{\varepsilon}}{\varepsilon} \mathrm{E}_{z1}^* \mathrm{E}_{z2} \right\} dA \tag{9}$$

where $\mathbf{E}_1(\mathbf{r},\omega)=(\mathbf{E}_{t1}, \mathrm{E}_{z1})$, and $\mathbf{E}_2(\mathbf{r},\omega)=(\mathbf{E}_{t2}, \mathrm{E}_{z2})$ are the transverse and longitudinal electric-field components of the modes of the original structure at frequency ω, and $\varepsilon(\mathbf{r})$ and $\tilde{\varepsilon}(\mathbf{r},z)$ are the dielectric constants of the original and perturbed structures, respectively. $\beta_1(\omega)$ and $\beta_2(\omega)$ are the propagation constants of the modes in the unperturbed structure. It is obvious that this integral is largest only when $\mathbf{E}_1(\mathbf{r},\omega)$ and $\mathbf{E}_2(\mathbf{r},\omega)$ have significant extent in the region of non-zero perturbation $\delta\varepsilon(\mathbf{r},z)=\varepsilon(\mathbf{r})-\tilde{\varepsilon}(\mathbf{r},z)$. In air-core PBGFs, perturbations to δε are greatest in the silica regions near the perimeters of the air holes.

The loss mechanism may be thought of in two parts. If the light is launched in a core mode the perturbations along the fiber can couple the light first into the surface modes and then into the extended modes. Due to the larger spatial extent of the surface modes and their localization in the silica regions, they are strongly coupled to the continuum of extended modes at all frequencies and so any light in the surface modes is quickly lost. It is only near to the avoided crossings that the core modes experience coupling to surface modes due to the large spatial overlap with the surface modes and the small δβ.

To demonstrate the first part of the process, namely the transfer of energy out of the core modes and into the surface modes, we plot coupling coefficients of the core/surface supermodes near the crossing shown in Fig. 3(b). We have assumed that δε is given by a ~2% perturbation of the air-filling fraction (from 94% to 92% AFF) of the real structure shown in Fig. 1(b). The fields were computed using a freely available software package that solves for the fully vectorial eigenmodes in a plane-wave basis [13]. Of the three modes shown in

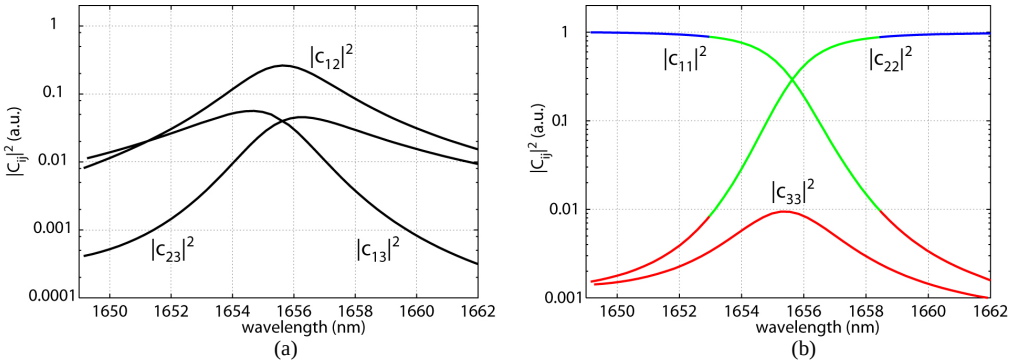

Fig. 6. (a) Coupling coefficients for a 2% change in air-filling fraction (AFF) for the modes shown in Fig. 3(b). The mode labels are given in Fig. 3(b). (b) The diagonal coupling coefficients indicate the impact of the perturbation on the propagation constants of the modes. The color scheme is the same as in Fig. 3(b).

#3956 - $15.00 US Received 2 March 2004; revised 28 March 2004; accepted 30 March 2004

Fig. 3(b), only modes labeled "1" and "2" participate strongly in the interaction. The third mode (labeled "3") is a fundamental core mode with a polarization that does not couple to the surface mode. Figure 6(a) quantifies this point showing that the maximum value of $|C_{12}|^2$ is almost an order of magnitude larger than $|C_{13}|^2$ or $|C_{23}|^2$. The calculation also predicts that $|C_{12}|^2$ is peaked at the avoided crossing where the two supermodes have a strong surface-mode component and that the coupling decreases rapidly away from the avoided crossing. The second plot in Fig. 6(b) shows the coefficients $|C_{ii}|^2$. In perturbation theory these terms give the first order correction to the propagation constant and are an indication of the overlap of the mode with the perturbation. From Fig 6(b) we see that when the supermodes are surface-mode-like they see significant impact from the perturbation but when they are core-mode-like the impact is reduced by nearly three orders of magnitude. Only when the perturbation impacts both modes "1" and "2" does the coupling occur as shown by $|C_{12}|^2$.

Although we have shown the coupling coefficients only for a perturbation in air-filling fraction, we believe that similar results would be obtained for other perturbations including scale changes and random perturbations. Of course, perturbations restricted to the core region have the most significant impact on coupling because of the overlap requirement with the core modes.

The final part of the process is to calculate the coupling between the surface modes and the extended modes. As carefree as we were with standard perturbation theory for the bound modes, we are much less confident of its utility in the case of extended modes. Moreover, the periodic boundary conditions of the plane-wave solver produce extended modes that are unphysical and we believe that these approximations to the true extended modes would not be adequate. That being said, we can only justify the coupling to the extended modes based on the fact that the surface modes have a much greater overlap with the extended modes and this overlap occurs mainly in the regions of high index where the structural perturbations are greatest.

In Fig. 7 we explicitly show the modal energy in the high-index regions for the modes of Fig 3. As expected, the core modes have very little energy in the glass while the surface modes typically have >50% of the energy in the glass. As shown in Fig. 7(b), the extended modes near the band gap also have a considerable amount of their energy in the glass, generally between 10% and 40% depending on which band edge, thus making the extended modes susceptible to structural perturbations that easily couple them to the surface modes and to other extended modes. These predictions of energy distribution are believed to be generally accurate but may be influenced by the periodic boundary conditions and the size of the supercell.

Though we have not rigorously calculated the surface-mode loss rate γ, we believe that we presented a plausibility argument that this loss rate is significantly higher than that due to

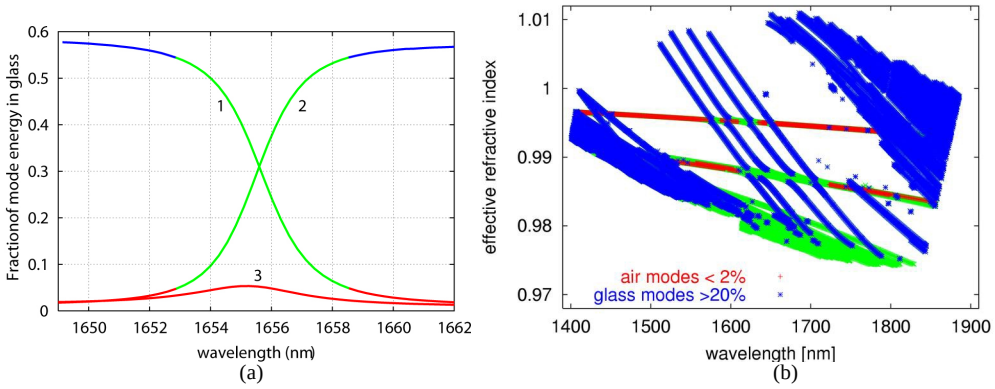

Fig. 7. (a) For the modes shown in Fig. 3(b), we plot the fraction of the mode energy contained in the glass, maintaining the color scheme of Fig. 3(b). (b) For the modes shown in Fig 3(a) we color-code the modes based on the fraction of the modal energy in the glass: >20%, blue; <2%, red; all others, green.

#3956 - $15.00 US Received 2 March 2004; revised 28 March 2004; accepted 30 March 2004

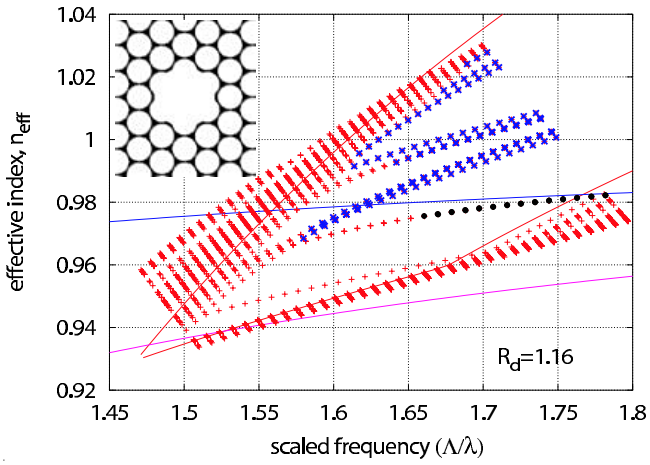

Fig. 8. (1 Mb) Movie of band-gap for varying core radii, R_d, showing the surface modes (blue) entering the gap and interacting with the core-guided modes (black). The continuum modes and modes whose character is neither core nor surface are colored red.

direct coupling between the core and extended modes. This is an important factor in understanding the nature of the surface-mode loss mechanism. We expect that for higher air-filling fractions and/or larger core diameters the coupling will decrease as the core modes become confined more tightly to the core region thus decreasing the overlap with the surface modes.

4. Fiber design without surface modes

The ultimate goal of this surface-mode study is to understand and reduce the impact of surface modes on the true air-core modes. In analogy to the surface modes seen in planar systems the first approach is to vary the position of the core surface with respect to the periodic lattice. This can be done by enlarging the circular air hole by cutting into the surrounding lattice. With the plane-wave code, we have modeled such an approach on a perfect lattice of air holes ($r=0.47\Lambda$) in silica. The results are shown in the movie in Fig. 8. As the glass is cut away

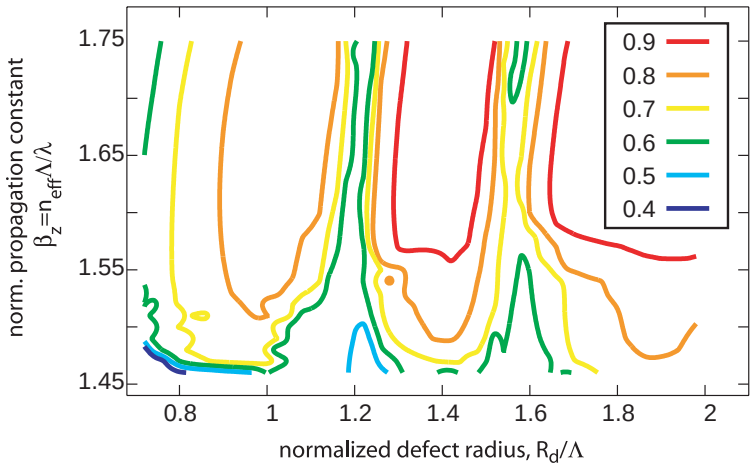

Fig. 9. Contour plot of fraction of core-confined energy *vs.* the propagation constant and the scaled defect radius R_d.

#3956 - $15.00 US
Received 2 March 2004; revised 28 March 2004; accepted 30 March 2004

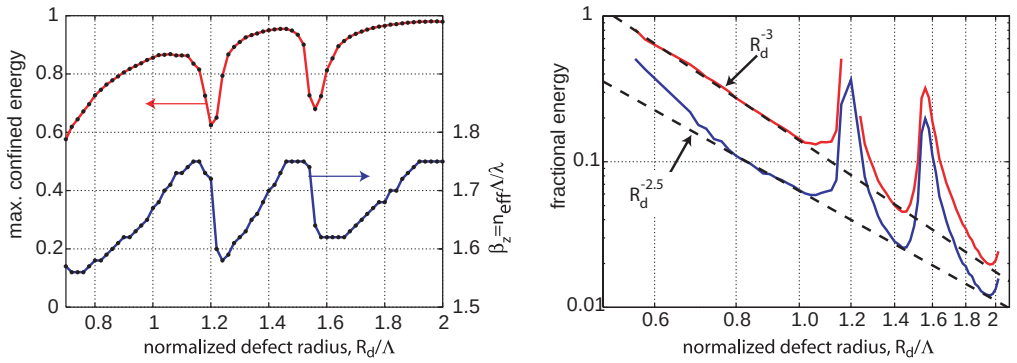

(a) (b)

Fig. 10. (a) The red curve is the fraction of core-confined energy *vs*. defect radius calculated for the most highly confined mode at each R_d in the contour plot from Fig. 9. The blue curve shows the β_z at which the mode appears. (b) A log-log plot of the fractional energy outside the core radius (red) and the fractional energy in the glass (blue) *vs*. defect radius for the same modes as shown in the left-hand plot. The dashed lines indicate that the while the energy outside of the core radius R_d scales inversely as the cube of R_d, the scaling for the energy in the glass is closer to $R_d^{-2.5}$.

from the core-cladding interface, the energies of some extended modes (2 modes for every lattice period on the surface [7]) are increased enough to push them into the band gap where they manifest as surface modes. This first occurs around R_d=1.06Λ. As the core radius increases, these surface modes continue through the gap interacting with the core modes as described in the preceding sections. At a radius of about 1.36Λ the surface modes have disappeared but they soon reappear at R_d=1.46Λ.

We can extract a more useful perspective by only looking at the mode with the highest energy in the core region. We show the results in Fig. 9 as a contour plot of fraction of core-confined energy *vs*. the propagation constant and the defect radius. This reveals plateaus of highly confined core modes near R_d=1.0Λ, 1.4Λ and 1.8Λ. A further simplification in Fig. 10(a) plots the highest core-confined energy for each defect radius. This clearly reveals PBGF designs that significantly reduce the impact of surface modes. The ideal single-mode design space is between R_d~0.9Λ and 1.1Λ, just below the defect radii often found in experimental fibers [2]. This structure and the corresponding core mode are shown in Fig. 11. The next optimal region is between R_d~1.35Λ and 1.45Λ but in this region the fiber becomes multimode, a property which is undesirable in most low-loss fiber applications.

Despite the presence of high-order modes, large-core PBGFs are one route to lower-loss fibers because of the increasing confinement of the mode to the air-core region. This is demonstrated by recent experiments in which losses of 1.7 dB/km were obtained in a large-

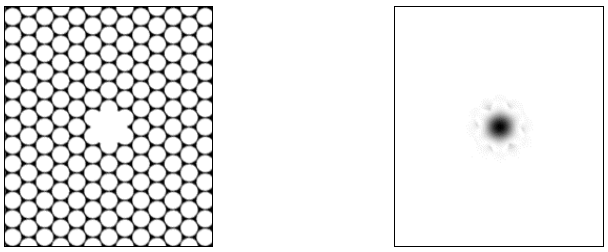

(a) (b)

Fig. 11. (a) Index profile of an improved PBGF design with r=0.47Λ and R_d=1.00Λ with no surface modes in the band gap. (b) Corresponding core mode at a scaled propagation constant of β_z=1.67.

#3956 - $15.00 US Received 2 March 2004; revised 28 March 2004; accepted 30 March 2004

core PBGF with R_d~2.5Λ [14]. Although the entire spectrum is not shown in Ref. 14, the sharpness of the surface-mode features is in agreement with the coupling and supermode arguments presented in Section 3. The lower loss is attributed to reduced mode coupling because less modal energy is contained in the glass. This suggestion is in agreement with the results shown in Fig. 10(b) in which both the energy outside of the core and the energy in the glass are plotted against the core radius for the fundamental core mode. Although the presence of the surface-mode coupling regions makes an exact power-law scaling hard to assess, the energy outside of the core appears to follow a $1/R_d^3$ dependence while the energy in the glass scales with the core radius to the power of -2.5.

We presented here the results for a fixed hole radius (r=0.47Λ) but the results are not very sensitive to air-filling fraction. We have studied air-filling fractions from 65% to 90% and the ranges of optimal and non-optimal core radii differ by only a few percent yielding plots that look nearly identical to those in Fig. 10. The air-filling fraction will have an effect on the core radius at which the fiber transitions between the traditional fundamental and higher-order core modes, but this radius happens to coincide with the appearance of surface modes, so the transition is poorly defined. Nonetheless for a large range of air-filling fractions, most of the first optimal design range defined above remains single-mode.

5. Summary

In conclusion we have argued that surface modes supported at the core-cladding interface lead to a loss mechanism unique to photonic band-gap fibers. At current loss levels, this effect dominates the loss in certain spectral regions and may contribute to loss over the entire transmission spectrum. The loss mechanism is well described by a supermode theory which predicts a number of Lorentzians loss peaks for the modes of the fiber. Though the net loss of a multimode PBGF may be in the range of 100 dB/km at wavelengths near the surface-mode crossings, the loss of individual core modes may be much greater in the vicinity of their coupling to surface modes. Finally, these surface modes may be avoided through appropriate design of the fiber core that includes fingers of silica protruding into the core region. It is anticipated that such a design will produce lower loss than current PBGFs and lead to single-mode performance.

#3956 - $15.00 US Received 2 March 2004; revised 28 March 2004; accepted 30 March 2004